Smart Receiver for Visible Light Communicatins: Design and Analysis

A. Burton, H. Le Minh, Z. Ghassemlooy, S. Rajbhandari and P. A. Haigh
Optical Communications Research Laboratory, NCRLab
Northumbria University, Newcastle-upon-Tyne, United Kingdom

***Abstract*—This paper presents the concept, design and analysis for a visible light communications receiver to guard against blocking and enhance mobility. Different geometrical shapes have been investigated, with two being chosen and analyzed in MATLAB for the received power and the root–mean–square (RMS) delay spread. The results show that the receiver is fully mobile within the test area and can handle data rates far greater than that offered by commercially available LEDs.**

***Index Terms*—LED, Visible Light Communications, Smart Receiver, Mobility, Shadowing, RMS Delay Spread**

I. Introduction

VISIBLE light communications (VLC) is an emerging technology that is gathering allot of interest from around the world. Predominantly VLC research involves increasing the data throughput, as the raw bandwidth of commercially available light emitting diodes (LEDs) are limited to only a few MHz [1-3]. Research into VLC mobility such as studies on blocking and shadowing effects are currently lacking; there is a myriad of investigations into the line-of-sight (LOS) case but not many into the non–LOS case which is more realistic when considering that the application will be implemented in future homes and an inherently LOS link will not always be available.

As a result of that, this paper will introduce the concept, initial design considerations and performance analysis of the proposed novel smart receiver design to guard against temporary line-of-sight (LOS) shadowing in a VLC system as well as mobility. The concept is to construct an optical antenna through an array of photodetectors (PD) capable of receiving light from all directions. Using the array of detectors, a hard decision will be made over which one of the PDs is to be used for the communications link, simply by measuring and comparing the received signal strength from each element. Thus when the predominant LOS link has been lost due to shadowing, the next best signal from the array will be selected to keep the communications channel open. The resulting non–LOS link however can be more than an order of magnitude lower in power than the LOS link [4, 5]; consequently upon detecting this the receiver will communicate to the VLC transmitter (via the RF uplink) requesting that the modulation depth of the data is increased, thus maximizing the total energy per bit/symbol to compensate. Once the LOS link has been restored, a subsequent request will be transmitted informing the transmitter to reduce the modulation depth.

978–1–4577–1719–2/12/ $26.00 ©

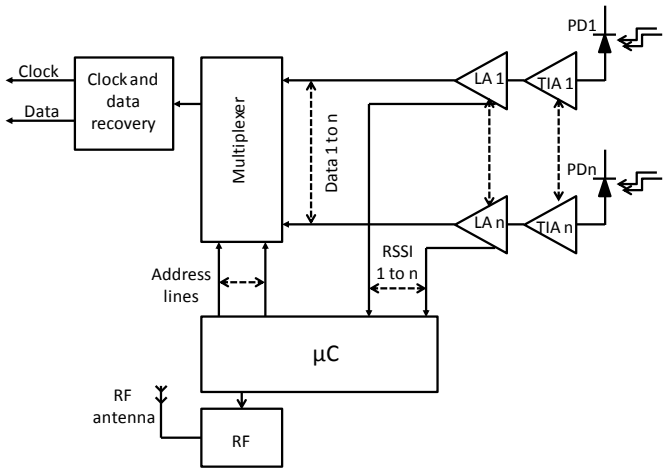

Fig. 1. Receiver block diagram

A block diagram for the receiving system is shown in Fig.1. PD1 through PDn of Fig.1 represent the array of photodetectors (with PD1 being the top LOS receiver) all being fed directly into their respective transimpedance amplifiers (TIA) and subsequent limiting amplifiers (LA). A measure of the received signal strength indication (RSSI) is coupled directly into the microcontroller (μC) where the decision is made over which input has the strongest signal. This information is translated to a binary address associated with the data inputs (LA1 to n) of the analogue multiplexer. The multiplexer output is sent directly to the clock and data recovery module. In the case where the signal on the LOS detector has been blocked, the μC can send a signal to the RF uplink unit requesting that the transmitter increase or decrease the transmission modulation depth.

II. Receiver Geometry

The design challenge is to create a mobile VLC optical antenna robust enough to mitigate the effects from temporary shadowing of the optical signal. A single detector will be employed at the top of the receiver for the LOS link, with an array of detectors situated around the sides of the receiver primarily used for the non–LOS reflected beam path. The receiver requires a 360° and 180° view along the $x-y$ axis and $x-z$ axis respectively (Fig. 2a). Therefore requiring minimum of three sides to the receiver. The fields of view (FOV) for each

of the side detectors need to satisfy the following condition:

$$FOV_{Side} = 360^\circ/n \tag{1}$$

where n is the number of side detectors. To fully utilize the FOV of the side detectors, each of the PDs will be tilted along the $x-z$ axis (Fig. 2b) thus:

$$a^\circ = FOV_{Side}/2 \tag{2}$$

The FOV of the top detector is given by:

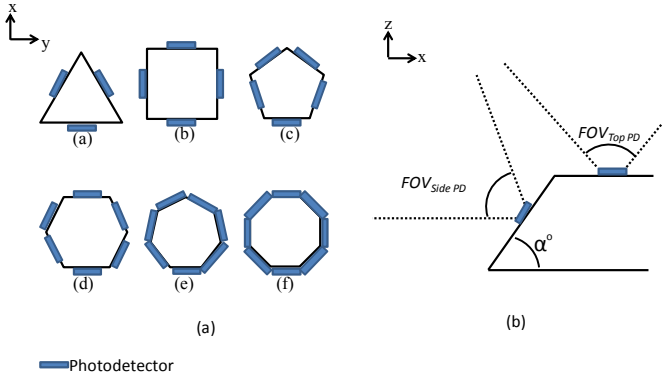

Fig. 2. (a) top view and (b) side view of receiver geometry

$$FOV_{Top} - 180^\circ - 2FOV_{Side} \tag{3}$$

Table 1 provides all the parameters calculated from equations 1-3. An overlap of the side and the top detectors occur for geometries a and b, hence the N/A entry in the FOV_{Side} column. Geometries a and b can therefore be discounted immediately due to the wide FOV, which can cause multipath inter-symbol interefece (ISI). Geometry e has also been eliminated simply due to the precision required for the FOV and tilt angle. Of the remaining candidates f has also been eliminated, reducing the number of detectors and complexity of the system. Therefore geometries c and d will be analyzed to determine the best performing layout.

TABLE I
CALCULATED GEOMETRIC ANGLES

Geometry	n	FOV_{Side}	Tilt angle (α)	FOV_{Top}
a	3	120°	60°	N/A
b	4	90°	45°	N/A
c	5	72°	36°	36°
d	6	60°	30°	60°
e	7	51.43°	25.715°	77.14°
f	8	45°	22.5°	90°

III. System Analysis

A. Introduction

MATLAB has been used to analyze the performance of the receiver geometries modeled within a small room ($2 \times 1.5 \times 1.2\ m^3$) with four walls and a single point Lambertian source in the centre of the ceiling. The received optical powers for the top and side detectors are investigated throughout all the positions of the receiving plane and include a single reflection from each wall. To estimate the available channel bandwidth the impulse response has been calculated for all positions with the RMS delay spread. This parameter provides a strong indicator of the maximum data rates achievable before the signal is degraded due to ISI.

B. Received optical communications power

For an optical link, the LOS DC channel gain is given by [4-6]:

$$H_{LOS}(0) = \begin{cases} \frac{(m+1)A}{2\pi D_d^2}\cos(\phi)^m T_s(\psi) g(\psi)\cos(\psi) \\ \quad \text{for } 0 \le \psi \le \Psi_c \\ 0 \quad \text{for } \psi > \Psi_c \end{cases} \tag{4}$$

where m is the Lambertian order of the LED transmitter and is given by the semi angle at half illuminance of the LED $\phi_{1/2}$ ($m = -\ln(2)/\ln(\cos(\phi_{1/2}))$, A is the size of the active area of the PD, D_d is the distance between the transmitter and receiver, ϕ is the angle of irradiance, ψ is the angle of incidence, $T_s(\psi)$ is the gain of an optical filter, and $g(\psi)$ is the gain of an optical concentrator. Ψ_c denotes the half width angle FOV at the receiver. The optical concentrator gain is give by [6]:

$$g(\psi) = \begin{cases} \frac{\eta}{\sin(\Psi_c)^2} & \text{for } 0 \le \psi \le \Psi_c \\ 0 & \text{for } \psi > \Psi_c \end{cases} \tag{5}$$

where η indicates the refractive index.

Therefore the received optical power from the LOS link can be computed by [7, 8]:

$$P_{rx} = H_{LOS}(0) P_{tx} \tag{6}$$

where P_{tx} is the transmit power

When considering the side received power, the DC gain of the reflected path is given by [9]:

$$dH_{ref}(0) = \begin{cases} \frac{(m+1)A}{2\pi^2 D_1^2 D_2^2}\rho dA_{wall}\cos(\phi)^m \cos(\alpha)\cos(\beta)\ldots \\ T_s(\psi) g(\psi)\cos(\psi) \quad \text{for } 0 \le \psi \le \Psi_c \\ 0 \quad \text{for } \psi > \Psi_c \end{cases} \tag{7}$$

where D_1 is the distance between the source and reflective area, D_2 is the distance between the reflective area and the receiver, ρ is the reflection coefficient, dA_{wall} is the small reflective region area, ϕ is the angle of irradiance to the reflective area, α and β are the angles of incidence and irradiance to and from the reflective area to the receiver respectively and ψ is the angle of incidence to the receiver.

Therefore the total received power at the detector is given by [9]:

$$P_{rx} = P_{tx} H_{LOS}(0) + \int_{walls} P_{tx} dH_{ref}(0) \tag{8}$$

Fig.3 and Fig.4 show the P_{rx} distribution throughout the receiving plane for the top PD for geometries c and d. with

TABLE II
SIMULATION PARAMETERS

Parameter	bfseries Value (unit)
Room x	2 $[m]$
Room y	1.5 $[m]$
Receiving plane to ceiling	1.2 $[m]$
LED half power angle ($\psi_{1/2}$)	70 [deg]
Wall reflection coefficient (ρ)	0.7
Number of reflections	1
Reflective area of wall	0.025 $[m^2]$
LED power	20 $[W]$
PD active area	15 $[mm^2]$
Detector FOV (FOV_{Top})	36 (c), 60 (d) [deg]
Detector FOV (FOV_{Side})	72 (c), 60 (d) [deg]
Tilt angle (α)	36 (c), 30 (d) [deg]
Optical filter gain ($T_s(\psi)$)	1
Optical concentrator gain ($g(\psi)$)	1

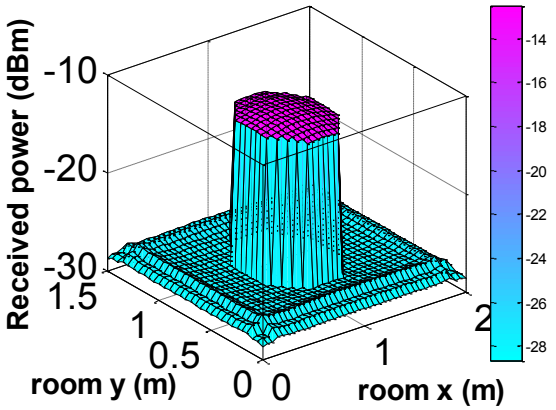

Fig. 3. Received power for the top detector in geometry c (max= -12.5 dBm, min= -28.65 dBm)

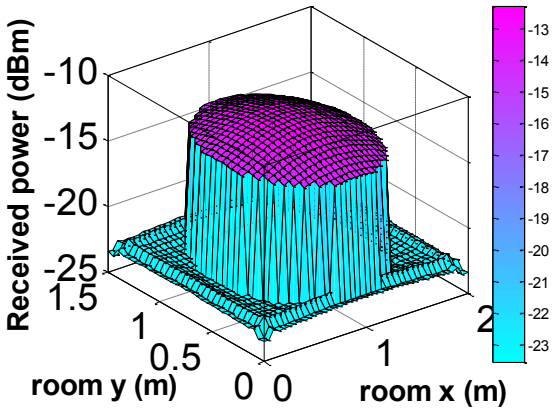

Fig. 4. Received power for the top detector in geometry d (max= -12.28 dBm, min= -23.55 dBm)

the parameters for the simulation outlined in Table 2. Fig.5 and Fig.6 show the received optical power profile for the side detectors. The result shown is for one of the detectors only

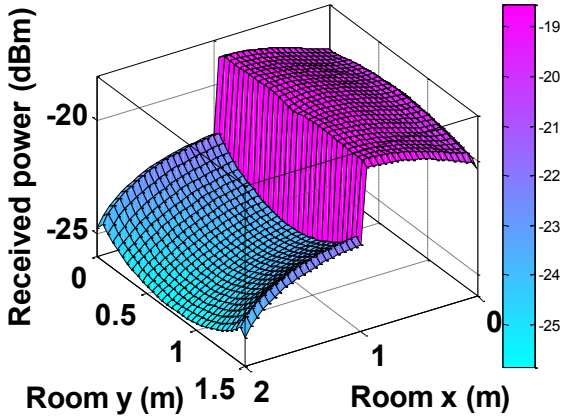

Fig. 5. Received power profile from a single side detector geometry c FOV= 72 deg tilt= 36 deg (max= -18.54 dBm, min= -25.85 dBm)

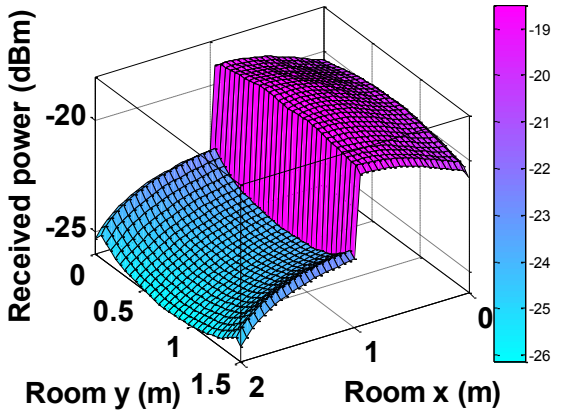

Fig. 6. received power profile from a single side detector geometry d FOV= 60 deg tilt= 30 deg (max= -18.52 dBm, min= -26.16dBm)

from geometries c and d. The configuration of the simulation is depicted in Fig.5. The plots illustrate that the detectors receive a relatively high power until they are moved passed the centre of the room and can no longer sustain the LOS link

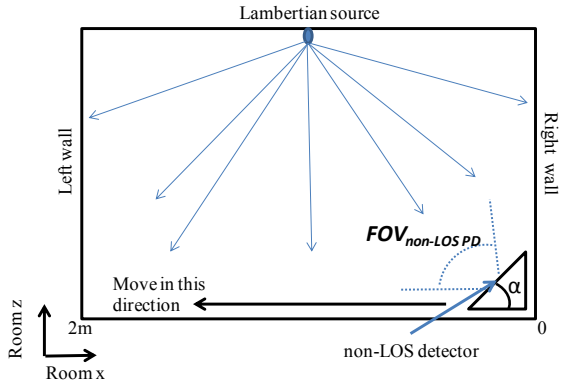

Fig. 7. Side detector simulation configuration

and the beam can no longer fall within the PD FOV. At this point the received optical power is entirely dependent upon the energy reflected from the walls. The distribution of the power in both Fig.3 to Fig.6 demonstrate that over the entire receiving surface, the received optical power is greater than the targeted -36 dBm level set by the optical sensitivity of the TIA (Analogue devices AD8015) used in the design.

C. Channel impulse response and RMS delay spread

Due to the multipath nature of the optical channel (LOS and reflections), the channel impulse response resembles a series of pulses. The delay profile or delay spread of pulses determines the dispersion of the channel and ultimately puts a constraint on the maximum channel capacity without the need for equalization. In particular, if the period of the data pulse is larger than the delay spread, ISI occurs at the receiver as two neighboring data pulses arrive at the same time. The maximum achievable data rate of the optical link is defined as 10% of the reciprocal of the RMS delay spread (τ_{RMS}) [10].

The RMS delay spread is gathered by first calculating the channel impulse response $h(t)$ distribution associated with the receiver throughout the receiving plane. This is achieved through calculating the P_{rx} from the LOS path with the associated time delay, and adding the power of proceeding received pulses from the reflected paths and their particular time delays. From $h(t)$ the τ_{RMS} can be computed by [11, 12]:

$$\tau_{RMS} = \sqrt{\frac{\int_{-\infty}^{\infty} (t-\tau_0)^2 h^2(t) \mathrm{d}t}{\int_{-\infty}^{\infty} h^2(t) \mathrm{d}t}} \tag{9}$$

where t is the time, and the mean delay τ_0 is given by[12]:

$$\tau_0 = \frac{\int_{-\infty}^{\infty} t h^2(t) \mathrm{d}t}{\int_{-\infty}^{\infty} h^2(t) \mathrm{d}t} \tag{10}$$

Fig.8 and Fig.9 show τ_{RMS} distribution throughout the receiving plane for the top detector of geometry c and d. It can be seen that τ_{RMS} is a minimum in the centre of the room where the light falling upon the detector is purely from the LOS path. As the detector moves closer to the walls of the room, reflections are detected causing the received impulse to spread and increasing τ_{RMS}. Maximum points are found close to the corners where reflections from multiple walls are detected. Likewise Fig.10 and Fig.11 depict τ_{RMS} for a side detector as in Fig.7. In this case the maximum τ_{RMS} occurs in the areas where both light from the LOS and non–LOS fall upon the detector. The spread then falls as the power from the LOS link decreases (after the halfway point along the x axis), only to pick up again in the areas where reflections from multiple walls meet. In each case the minimum channel capacity for the top detectors is above 200 Mbps (corresponding to a τ_{RMS} of 0.5 ns), showing that channel induced ISI will not be the limiting factor to the system as the data rate range of 200 Mbps is much greater than the available white LED modulation bandwidth. And for the side detectors there is a

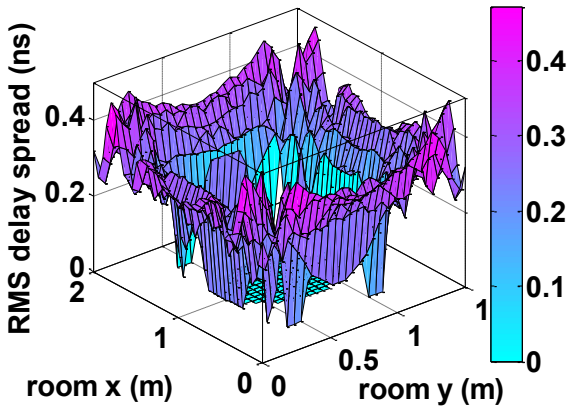

Fig. 8. RMS delay spread for the top detector of geometry c (max= 0.47 ns)

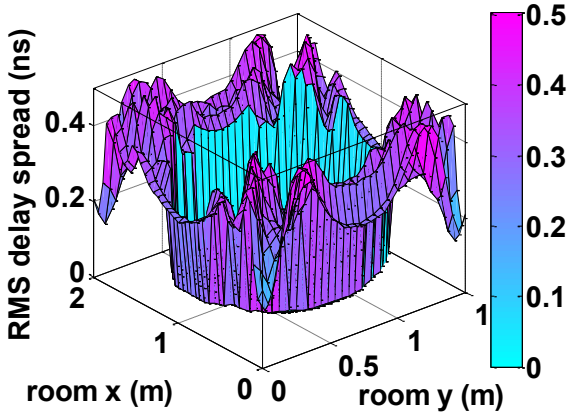

Fig. 9. RMS delay spread for the top detector of geometry d (max= 0.49 ns)

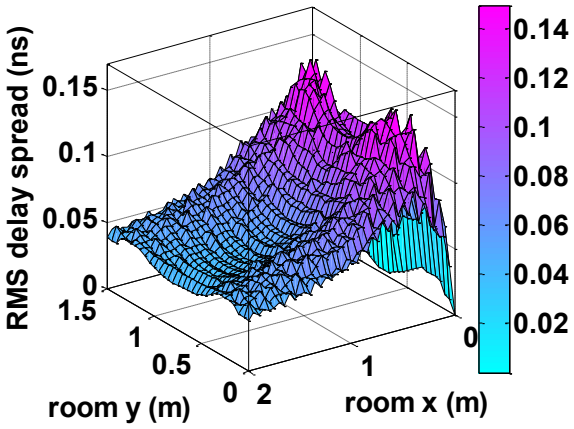

Fig. 10. RMS delay spread for the side detector of geometry c (max= 0.27 ns)

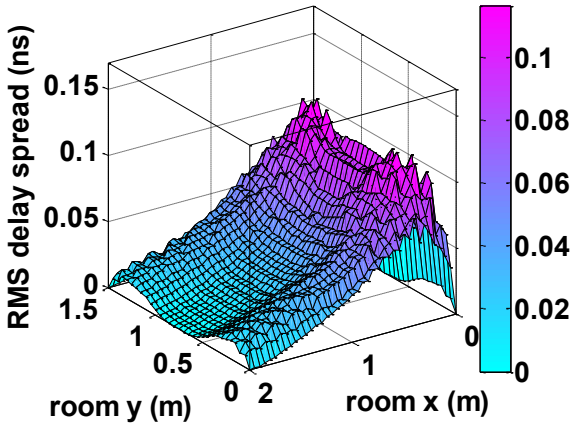

Fig. 11. RMS delay spread for the side detector of geometry d (max$= 0.22$ ns)

minimum channel capacity of 666 Mbps (corresponding to a τ_{RMS} of 0.15 ns). Hence both geometries show the ability to perform within the required channel bandwidth limitations.

IV. Conclusion

The analysis has shown that both geometries c and d behave well within the simulated environment. The received optical power is greater than that required by the receiver (-36 dBm), even when only the reflected path is taken into consideration. The RMS delay spread has also indicated that ISI will only occur at bit rates far greater than the LEDs allow. Both geometries for the side detectors behave almost identically as their tilt and FOV angles are nearly the same (only a few degrees different). However geometry d with almost double FOV of the LOS detector when compared with c, is capable of covering a far greater area thus giving it an inherent advantage when it comes to robustness against temporary shadowing or blocking. Geometry d also has the advantage of the FOV for all the detectors are equal, reducing the complexity of the system build through cloning.

Acknowledgment

The author A. R. Burton would like to acknowledge the financial support received from the school of Computing, Engineering and Information Sciences at the University of Northumbria at Newcastle to carry out this research. This work is supported by the EU Cost Actions of IC0802 and IC0110.

References

[1] H. Le Minh, D. O'Brien, G. Faulkner, Z. Lubin, L. Kyungwoo, J. Daekwang, and O. YunJe, "High-Speed Visible Light Communications Using Multiple-Resonant Equalization," Photonics Technology Letters, IEEE, vol. 20, pp. 1243-1245, 2008.

[2] H. Le Minh, D. O'Brien, G. Faulkner, Z. Lubin, L. Kyungwoo, J. Daekwang, O. YunJe, and W. Eun Tae, "100-Mb/s NRZ Visible Light Communications Using a Postequalized White LED," Photonics Technology Letters, IEEE, vol. 21, pp. 1063-1065, 2009.

[3] H. Le Minh, D. O'Brien, G. Faulkner, L. Zeng, L. Kyungwoo, J. Daekwang, and O. YunJe, "80 Mbit/s Visible Light Communications using pre-equalized white LED," in Optical Communication, 2008. ECOC 2008. 34th European Conference on, 2008, pp. 1-2.

[4] T. Komine and M. Nakagawa, "Fundamental analysis for visible-light communication system using LED lights," Consumer Electronics, IEEE Transactions on, vol. 50, pp. 100-107, 2004.

[5] K. Fan, T. Komine, Y. Tanaka, and M. Nakagawa, "The effect of reflection on indoor visible-light communication system utilizing white LEDs," in Wireless Personal Multimedia Communications, 2002. The 5th International Symposium on, 2002, pp. 611-615 vol.2.

[6] C. Jae Hyuck, K. Sung Wan, and K. Jin Young, "Influence of optical path difference on visible light communication systems," in Communications and Information Technology, 2009. ISCIT 2009. 9th International Symposium on, 2009, pp. 1247-1251.

[7] H. Elgala, R. Mesleh, and H. Haas, "Indoor broadcasting via white LEDs and OFDM," Consumer Electronics, IEEE Transactions on, vol. 55, pp. 1127-1134, 2009.

[8] T. Komine, L. Jun Hwan, S. Haruyama, and M. Nakagawa, "Adaptive equalization system for visible light wireless communication utilizing multiple white LED lighting equipment," Wireless Communications, IEEE Transactions on, vol. 8, pp. 2892-2900, 2009.

[9] Y. Alqudah, M. Kavehrad, and S. Jivkova, "Optical wireless multispot diffusing: a MIMO configuration," in Communications, 2004 IEEE International Conference on, 2004, pp. 3348-3352 Vol.6.

[10] T. S. Rappaport, Wireless Communications: Principles and Practice vol. Vol 2. New York: Prentice Hall, 2001.

[11] [M. D. Higgins, R. J. Green, and M. S. Leeson, "Genetic algorithm channel control for indoor optical wireless communications," in Transparent Optical Networks, 2008. ICTON 2008. 10th Anniversary International Conference on, 2008, pp. 189-192.

[12] J. B. Carruthers, S. M. Carroll, and P. Kannan, "Propagation modelling for indoor optical wireless communications using fast multi-receiver channel estimation," Optoelectronics, IEE Proceedings -, vol. 150, pp. 473-481, 2003.